

# Unsteady computational simulation of the flow structure of an isolated wheel in contact with the ground

P.R.K. Dassanayake<sup>1</sup>, D. Ramachandran<sup>1</sup>, L. Salati<sup>1,2</sup>, T.J. Barber<sup>1</sup>, G.C. Doig<sup>1</sup>

<sup>1</sup>School of Mechanical and Manufacturing Engineering, University of New South Wales, Sydney, NSW 2052, Australia

<sup>2</sup>Department of Mechanics, Politecnico di Milano, Milano 20133, Italy

## Abstract

The flow around an isolated wheel, as in a Formula 1 car, is complex and yet often simulated using Reynolds Averaged Navier Stokes models. Given the transient, three-dimensional nature of the flow field, LES (Large Eddy Simulations) and/or DES (Detached Eddy Simulations) are more appropriate. In this work, an exposed rotating wheel in contact with the ground has been modelled using unsteady RANS (Reynolds Average Navier Stokes), LES and DES. The comparison allows the effect of the unsteady RANS approximation to be appreciated by drawing conclusions from observing the flow field around the wheel, giving special attention to the vortices generated. The LES/DES models reveal details of the transient flow field that were not apparent from unsteady RANS simulations.

## Introduction

The complex flow field and forces around an isolated wheel are of interest to the motor racing industry, through potential performance increases and also to the automotive community due to the possible economic benefits. Analysing the airflow can lead to better understanding the influence of the wheel rotation on the wake region. This contributes to better models of road vehicles.

In certain circumstances such as Formula 1, wheels play a dominant role in the aerodynamic behaviour of the vehicle. Understanding the wake structure around isolated wheels leads to better controlling the wake dynamics, increasing down force and improving brake/engine cooling [2]. For open-wheeled racing cars, the wheel contributes to some 40% of the total drag and therefore gives rise to considerable complexity to flow around other structures of the vehicle [1].

The benchmark experimental work well known in the field of isolated wheels is that of Fackrell and Harvey [5]. The experimental work confirmed previous results obtained both by Cogotti [5] and Stapleford and Carr [9]. The analyses observed the behaviour of airflow around a variation of wheel types altering the wheel width, shape and tread pattern with special attention given to the interaction of a rotating wheel in contact with the ground.

RANS simulations utilising the two-layer RNG  $k-\epsilon$  turbulence model were able to compute aerodynamic forces and surface pressures that agree with experimental

work [5] however the simulation behaved poorly around regions of large separation and strong unsteadiness, such as the immediate wake region of the wheel [3] and as a result it is not used in the industry to observe the flow field. These simulations were done on the wheel geometry 'B2' referred to by experimental work [5].

## Wheel geometry

To compare with experimental data, the geometry was chosen to be the 'A2' configuration referred to by Fackrell and Harvey [5]. The wheel has a diameter of  $d=415.9\text{mm}$ , a shoulder width of  $b=185.4\text{mm}$  and the hub is similar to that found in literature except the edge was simplified. The contact patch region of the wheel with the ground is a vital area for computational analysis since it affects the wake airflow behaviour. Fackrell and Harvey [5] observed a peak in surface pressure on the wheel immediately upstream of the contact between the wheel and the ground. The pressure peak is subjected to a 'jetting' effect observed when the boundary layers on the wheel and the moving ground are forced towards the contact line between the two. The flow then emerges as a jet at the edges of the wheel.

## Grid description

The grid was generated using the commercial software STAR-CCM+ by employing the trimmer meshing technique to generate the volume mesh. A cylindrical shaped volumetric control around the wheel and a rectangular shaped volumetric control at the wheel wake were set up to better capture the flow features in these regions. Two grids were generated; one labeled coarse mesh (3.48million cells) and the other labeled fine mesh (6.97million cells).

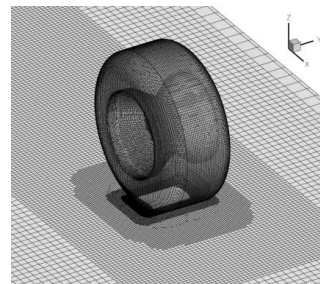


Figure 1: Volume mesh around the wheel and moving ground

A Grid Convergence Index (GCI) was computed to quantify the errors associated when using the coarse mesh compared to the fine mesh. Based on lift and drag

coefficients the GCI was found to be 1.7% and 2.7%, respectively. Therefore, only a small error is associated compared to the computational cost involved in running simulations using a finer mesh. Therefore, all results presented in this paper are based on the coarse mesh solution. This grid has a  $y^+$  value of less than 1 all around the wheel except at the interface with the contact patch where a  $y^+$  value of 2.7 was obtained.

### Computational method

Star CCM was used as it generates high-quality but efficient cartesian background meshes with boundary layer prisms for capturing attached shear layers. The meshes generated were then solved with the commercial code FLUENT 13.0 to take advantage of available parallel computing resources. The second-order, upwind discretization scheme was used for the pressure, momentum, turbulent kinetic energy and specific dissipation terms of the Navier Stokes equation for the unsteady RANS and DES methods. However a bounded central differencing scheme was implemented for the LES model. The SIMPLEC algorithm was implemented for the pressure-velocity coupling.

The inlet was set to a constant velocity of 18.6 m/s. Since the boundary was modelled to be open, the outlet was set to atmospheric conditions. The floor of the test section was modelled as an accumulation of a moving ground and a no slip wall. This was done to keep consistency with the experimental procedure. The moving ground had the same velocity as the inlet. The walls of the wind tunnel were set to be zero shear walls. The inlet and the outlet turbulence intensity were set to 0.2% with the turbulence length scale at 0.04m, roughly 10% of the diameter of the wheel. The surface of the wheel was set as a rotating boundary with no slip. The rotational velocity of the wheel was 89.4rad/s

The domain boundary was designed to be  $20d=8.3m$  long, width 1.2m and height 1.5m. The wheel was placed in the middle, with  $10d=4.2m$  clearance to the inlet and outlet. The moving road is of  $5d=2.1m$  magnitude on either side of the centre line of the wheel with the same span as the test section.

The two equation,  $k-\omega(SST)$  turbulence model was implemented in the unsteady RANS simulations. The specific turbulence model was chosen because of its near wall modelling ability. The DES model utilised the one equation Spalart-Allmaras (S-A) model. It was chosen because of its common use in the industry to model road vehicle flows [6]. It is also an adequate model in being able to capture vortex shedding close to the wall. The WALE sub grid scale (SGS) model was used for the LES simulations. The WALE constant was set to 0.325 for the simulation.

All three unsteady simulations was computed with a 0.00025s time step. This time step chosen based on analysing different time steps and running power

spectrum analysis on the lift and drag coefficients of the wheel. From the power spectrum analysis, distinct peaks were searched for regarding the different vortices shed from the wheel and the best time step was chosen based upon the time step that yielded the least amount of noise around the frequency peaks. The time step was validated by the work carried out by Salati [8] on a mesh of similar density.

### Results and discussion

To compare with experimental data [5], the surface pressure coefficients were computed around the circumference of the wheel. The unsteady simulation results were time-averaged to compare with the steady simulations and the experimental data.

A sharp pressure peak is observed when the flow approaches the line of contact. This corresponds with the ‘jetting’ phenomenon [5]. As seen in figure 2, the computed pressure peak just before the line of contact by the three different simulations are within 6.9% of each other;  $C_p=1.62$  (unsteady RANS),  $C_p = 1.73$  (DES) and  $C_p = 1.74$  (LES). These pressure peak results show a maximum 39% correlation with the experimental data [5]. A minor negative pressure peak is observed in the unsteady RANS and DES simulation immediately after the line of contact (refer to figure 2). Fackrell and Harvey [5] theoretically predicted this as the ‘jetting’ effect in reverse however they were not able to observe it in the experimental data. McManus [6] observed this negative pressure but at a much higher magnitude. The magnitudes of the negative pressure peaks are  $C_p = -0.45$  (unsteady RANS) and  $C_p = -0.44$  (DES).

Except for LES, the separation of the flow shows good agreement with experimental data. This is due to the LES formulation requiring high resolution mesh to predict flows in boundary layer region with low Reynolds number. Both unsteady RANS and DES predict separation at around  $280^\circ$ , which is in excellent agreement with experimental data [5]. LES predicted separation further downstream at  $272^\circ$ .

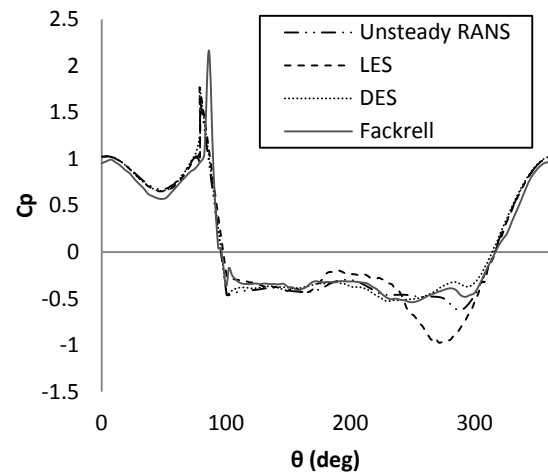


Figure 2: Surface pressure coefficient around the centreline of the wheel

The variation in the position of the separation point and the magnitude of the pressure at the top of the wheel is discussed by Fackrell and Harvey [5] being subject to the wheel edge profile, however it was deduced that the observed variation can be attributed to the deficiencies in the boundary layer region

*Upper wake Region:* Figure 3 shows the upper wake region on the trailing edge of the wheel at an angle of  $60^\circ$  for the different methods of simulation. As it can be seen, the flow separates from the wheel on the upper surface of the wheel on all three occasions. In the DES and unsteady RANS simulations, the separated flow forms an arched shaped vortex, in consistent with published work [5]. This is because the DES simulation behaves as a S-A unsteady RANS simulation near the walls. The arched vortex has a width approximately the same as the wheel which keeps in agreement with that observed by McManus [6]. In the LES simulation, the upper wake region forms a pair of vortices that rolls into each other. This agrees with Cogotti's [5] work where the trailing vortex in the upper wake behaved as a pair.

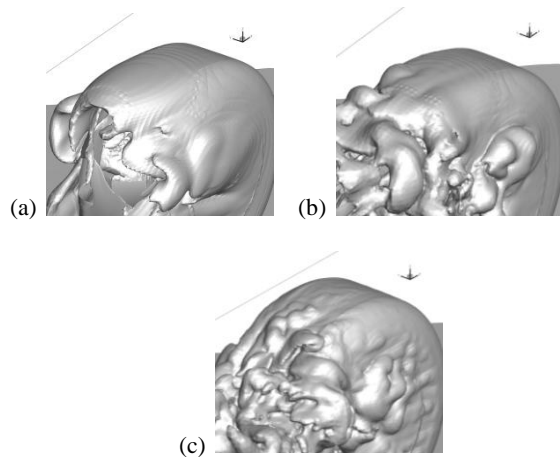


Figure 3: Isosurface of vorticity magnitude ( $500s^{-1}$ ) in the upper wake region: (a) unsteady RANS, (b) DES and (c) LES

*Lower separation region:* In all three unsteady simulations shown in figure 4, near the line of contact at the lower separation region of the wheel, the flow emerged in a sideward direction from under the front of the wheel. This flow correlates with the surface pressure coefficients seen in Figure 2, where a positive pressure peak is seen before the forward line of contact. In the unsteady RANS simulations, the flow emerging from the hub is not mixing with the flow in the lower separation region. This is in agreement with what McManus [6] observed. The LES and DES simulation however shows flow interaction between the hub and the lower separation region. This causes the vortex emerging from the lower separation region to break down and spread wider from the wheel (zone 4 in figure 5). As it can be seen in figure 6, the hub vortices are more prominent in the upper quadrant and once the vortices escape the hub (zone 1 in figure 4); the rotation of the wheel causes the

vortices to interact with the flow in the lower separation region.

*Lower wake region:* The pair of vortices formed from the upper wake region in the LES simulation becomes more prominent further downstream of the wake region (zone 3 in figure 5).

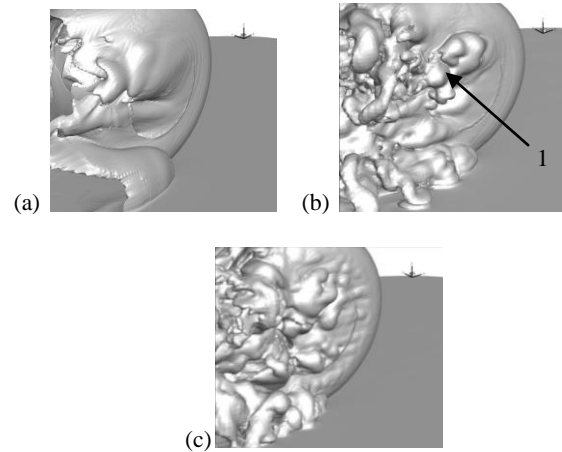
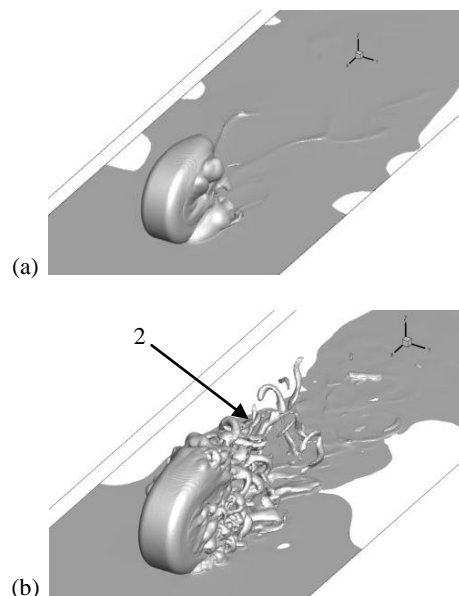


Figure 4: Isosurface of vorticity magnitude ( $500s^{-1}$ ) in the lower separation region: (a) unsteady RANS, (b) DES and (c) LES

In the DES simulation, the vortices from the hub interact with the upper wake region and results in discontinued vortices that roll upon themselves (zone 2 in figure 5). This discontinuity is observed past  $1d$  distance from the trailing edge of the wheel. The near wall detail in the vortices is more prominent in the LES simulation further downstream from the wheel. The unsteady RANS simulation is not able to show the same level of detail as seen by McManus [6]. The counter-rotating longitudinal vortices



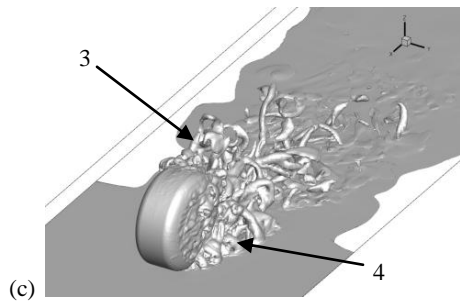


Figure 5: Isosurface of vorticity magnitude ( $500s^{-1}$ ) in the lower wake region: (a) unsteady RANS, (b) DES and (c) LES

**Hub region:** Figure 6 shows cross sectional vorticity contours at the centre plan of the wheel. It can be seen in figure 6 that in all three unsteady simulations, the hub vortices are more prominent in the upper quadrant of the hub. The unsteady RANS simulation shows the right side hub to produce a larger vorticity where as both LES and DES show a larger vorticity formed in the left side hub. The vorticity magnitude in the unsteady RANS simulation near the hub wall is lower in magnitude however more consistent. This is because the unsteady RANS simulation is averaging it and therefore is not able to capture the same level of detail as LES and DES, which is able to show the small vortices that are present in the inner wall of the hub.

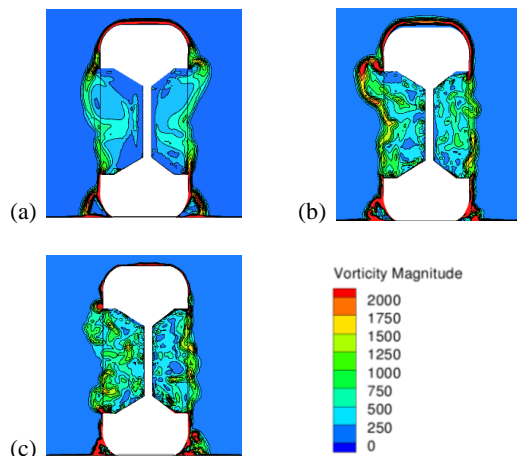


Figure 6: Cross sectional (centre of the wheel) vorticity magnitude ( $500s^{-1}$ ): (a) unsteady RANS, (b) DES and (c) LES

### Conclusion

The computational simulations to observe the flow field of an isolated rotating wheel show that LES and DES are able to capture more detail of the wake region than unsteady RANS. Unsteady RANS simulation is adequate to show the surface pressure coefficient variation. All three unsteady simulations show adequate comparison to experimental work [5] near the line of contact. In contrast with McManus' [6] work where a greater positive and negative pressure is observed immediately before and after the line of contact subject to the 'jetting' effect [5].

The trailing vortex in the upper wake region for the unsteady RANS and DES model form an arch shaped vortex, as also seen by McManus [6]. Similar results

were observed by unsteady RANS and DES since DES behaves as a S-A unsteady RANS simulation near walls. The LES simulation however forms a pair of trailing vortices in the upper region of the trailing edge of the wheel, which agrees with the theoretical considerations by Cogotti [4]. The DES and LES simulations both shows the flow from the region near the rear line of contact interact with the vortices formed from the hub due to the rotation of the wheel. The DES simulation show the trailing edge vortices in the lower wake region show discontinuity once they are of adequate distance from the trailing edge of the wheel. The vortices generated within the hub region of the wheel are prominent in the upper quadrant of the hub. In conclusion, the LES/DES simulation show more detail with regards to the flow field and shows greater consistency with experimental data. LES showed greater detail in the flow field however it is computational more expensive than DES.

### References

- [1]. AGATHANGELOU, B. G. M. 1998. Aerodynamic Design Considerations of a Formula 1 Racing Car. *SAE International Congress and Exposition*. Detroit, Michigan.
- [2]. AXERIO, J., LACCARINO, G., ISSAKHANIAN, E., LO, K., ELKINS, C. & EATON, J. 2009. Computational and Experimental Investigation of the Flow Structure and Vortex Dynamics in the Wake of a Formula 1 Tire. *SAE World Congress*. Detroit, Michigan.
- [3]. AXON, L., GARRY, K. & HOWELL, J. 1998. An Evaluation of CFD for Modelling the flow Around Stationary and Rotating Isolated Wheels. *SAE World Congress*. Detroit, Michigan.
- [4]. COGOTTI, A. 1983. Aerodynamic characteristics of car wheels. *International Journal of Vehicle Design, Technological Advances in Vehicle Design Series*, 173-196.
- [5]. FACKRELL, J. E. & HARVEY, J. E. 1974. *The Aerodynamics of an Isolated Wheel Rotating in Contact With the Ground*. PhD, University of London.
- [6]. MCMANUS, J. & ZHANG, X. 2006. A Computational Study of the Flow Around an Isolated Wheel in Contact with the Ground. *Journal of Fluids Engineering*, 128, 520-530.
- [7]. RAMACHANDRAN, D. 2012. *Complex Flow around an Exposed Rotating Wheel*. Bachelor of Mechanical Engineering, University of New South Wales.
- [8]. SALATI, L. 2012. *Detached Eddy Simulations on a fully exposed rotating wheel in contact with a moving ground*. Masters, University of New South Wales.
- [9]. STAPLEFORD, W. R. & CARR, G. W. 1970. Aerodynamic Characteristics of Exposed Rotating Wheels. *MIRA Technical Paper*. Nuneaton, UK.